Online state of charge estimation for a vanadium redox flow battery with unequal flow rates

Alejandro Clemente*, Andreu Cecilia and Ramon Costa-Castelló

Institut de Robòtica i Informàtica Industrial, CSIC-UPC, Llorens i Artigues 4-6, 08028 Barcelona, Spain

alejandro.clemente.leon@upc.edu, andreu.cecilia@upc.edu, ramon.costa@upc.edu

Abstract This study presents an observer-based methodology to estimate, in real-time, the state of charge of a Vanadium redox flow battery. Different from the available results in the literature, this work presents a new estimator that distinguishes between the concentration in the tank and cell parts of the system. Moreover, it presents an estimation of the state of charge that can deal with both balanced and unbalanced situations. The model used for the observer design is a nonlinear electrochemical model. A nonlinear observer is proposed, designed and validated through simulation and in an experimental prototype.

Keywords: Redox flow battery, State of Charge, nonlinear observer

1 Introduction

In the current energy situation where energy storage systems (ESS) have become one of the greatest needs, the search of a large-scale, long-life and low-cost storage systems has become crucial. Indeed, an ESS that meets these requirements could be implemented in large-scale facilities where energy generation can be intermittent, as is the case of solar and wind plants.

Within this scenario, redox flow batteries (RFB) have become one of the most promising solutions [4]. Its operating principle is based on the use of four different species separated two by two by a membrane. These species are dissolved in a liquid, known as electrolyte, that is transported to an electrochemical cell where the redox reaction takes place. Depending on the flow of electrons from the charge or discharge current, the species concentration will vary, according to the phenomena of oxidation and reduction.

Although there exist different types of RFB, depending on the materials and the nature of the chemical species, all of them share similar components and structure, as it can be seen in Figure 1. First, the RFB presents the tanks that contain the electrolytes. Depending on the side of the system, it is possible to differentiate between catholyte and anolyte. Second, the RFB includes a set of pumps, that allow the injection of the electrolyte through the entire system, closing the tank-cell cycle. Finally, the electrochemical cell serves as an enclosure where redox reactions take place.

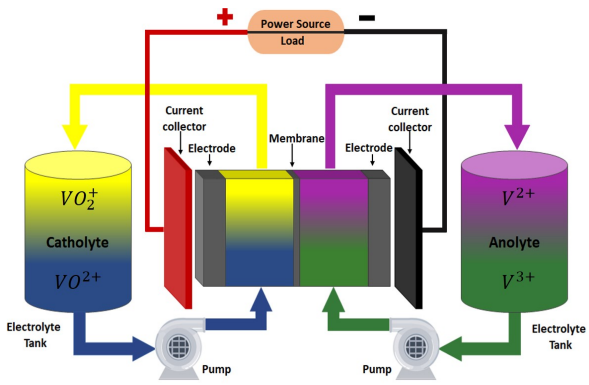

Figure 1: Vanadium redox flow battery scheme with its main components and particular color of each species.

Despite its low-energy density (compared to other ESS) [14], which takes values from 15 to 40 Wh·l^{-1}, its flexible and modular design, among other characteristics, make the RFB a good option for large-scale facilities. On the one hand, the power is determined by the dimension and number of cells that can be put in series conforming the stack. On the other hand, the capacity depends exclusively on the volume of the tanks where the electrolytes are stored. Therefore, as the capacity is directly related with the tank volumes, RFB are suitable for large-scale energy applications that may have large areas to contain large tanks, as is the case of power plants.

The main distinction between different RFB sys-

tems is given by the nature of the active species that conform the electrolytes. In this way, it is worth highlighting the all-vanadium redox flow battery (VRFB) developed by professor Skyllas-Kazacos [29]. The main advantage of a VRFB is that all species are oxides of vanadium, guaranteeing that a possible mixture of electrolytes due to the transport phenomena through the membrane will not cause any damage. The anolyte is composed by the existent vanadium species V^{2+} and V^{3+} and the catholyte by the vanadium valences V^{4+} and V^{5+} that on the nature, exist as the oxides VO^{2+} and VO_2^+, respectively.

Although extensive analysis of different aspects concerning the VRFB has been done during all these years, control techniques and internal variable estimators are still an open area of study. Specially, within the control field, one of the most important challenges corresponds to determine the state of charge (SOC) of a RFB [26].

The SOC gives information about the energy that is stored in the system, being directly related with the proportion of species contained on it. As in any type of battery or ESS, knowledge of the SOC is essential to analyze the correct system operation [11], being also a variable used for the design of optimal-flow controllers [2, 12]. As the SOC can be directly computed from the species concentration, one of the major fields of study consists on finding possible sensors to measure these concentrations in real-time. Currently, most of the physical properties used to compute the SOC are the electrolyte color, viscosity or conductivity [32]. However, none of them have yielded encouraging results. For the case of the color analysis of a VRFB, each vanadium species has a particular color corresponding to the ones shown in Figure 1. However, once the species are dissolved in sulfuric acid, the electrolyte turns almost black and is hardly possible to extract color information [31]. Viscosity or conductivity measures require offline analysis, due to the fact that is very difficult to differentiate between valences of the same species in real time. Therefore, either for their inaccuracy or they intrusivity, these measures are not the best solution for the real-time estimation of the SOC.

Considering the lack of sensors that allow obtaining accurate measurements in real time, the use of observers is an attractive alternative [3]. This technique has been used to solve monitoring problems in similar electrochemical systems [8, 9] using simple to measure signals. Within the field of lithium batteries, lot of research has been done in order to choose the appropriate variables to measure, which commonly are the voltage, current and temperature [38]. Specially, there exist some observers intended to estimate the SOC even in situations of sensor uncertainty, as it is presented in [39]. Measurement noise is another important factor that must be taken into account when designing an observer, being essential to achieve a good performance, as has been studied in the literature [37]. For that reason, previously to the implementation of a SOC estimator, it is necessary to choose the proper sensors, seeking a trade-off between simplicity in their implementation, reliability and richness in terms of information for the estimation.

Among all the possible variables to be used to infer the SOC value for VRFB, voltage and temperature stand out. Both measures depend on the species concentrations inside the cell, existing numerous models that relate them [18].

However, it should be noted that while the influence of the concentrations in the voltage value are decisive, it is not so for the temperature where ohmic losses have a much greater influence. Therefore, the open-circuit voltage (OCV) characterized by the Nernst equation is the most widely used variable chosen for the development of VRFB observers [34].

In the literature there are different observers that have been developed to estimate the SOC for VRFB. Nevertheless, most of them make a set of assumptions to simplify the model that are hardly met on reality. One of the main assumptions is to consider that the electrolyte flow rate is large enough so that the tank and cell concentration is the same one, thus allowing to express the OCV as a function of the SOC. Moreover, within this assumption, it is also assumed that the flow rate is the same for both parts of the system. Using these hypothesis, Skyllas-Kazacos has presented different estimators. For only SOC estimation, an Extended Kalman Filter (EKF) is presented in [44] and a Sliding Mode Observer (SMO) considering a reduced model with only two states is presented in [10]. For both SOC and SOH estimation, SMO [42] and an adaptive estimation based on an online identified battery model [41] have been presented.

Another type of estimators that also appears frequently in the literature use equivalent circuit models [13]. Other examples are the case of [43] and [45] which present a dynamic electric model to estimate the SOC considering that concentration in cell and tank are exactly equal. For all these cases, the effect of the flow rate is neglected, which can lead to long-term observer malfunction.

Previous VRFB SOC estimation works assume that the VRFB operate at very-high flow rates and that the flow rate is equal in both VRFB pumps. These assumptions implies that cell and tanks concentrations are almost the same. Unfortunately, these hypotheses are not very realistic in most real VRFB. On the one hand, very high flow rates may not be beneficial for the pumps, generating more losses. There are different studies that analyse the benefits of variable flow rates

depending on the operating conditions, maximizing the battery efficiency when cell and tank concentrations are different [15]. On the other hand, for an optimal operation it is convenient to adapt the flow rates to the operating conditions. Equal flow rates are very convenient when the VRFB is balanced. However, RFB have a natural tendency to system imbalance due to the ion transport caused by different phenomena such as diffusion, migration or convention. Operating the system at different flow rates is a strategy to reduce the system imbalance phenomena [16].

Considering these limitations, this paper presents a SOC estimator based on a nonlinear electrochemical model. The model considered differentiates between cell and tank species concentration, presenting new definitions of the SOC that differ from those commonly used in the literature where the SOC is assumed to be the same in both sides of the system. For that reason, the SOC is expressed in terms of available mass of species, differentiating between anolyte and catholyte sides of the system. Within this scenario, it is essential to choose a good observer strategy for nonlinear systems. The use of High-Gain Observers (HGO) [6] and Sliding Mode Observers (SMO) [7, 22] are one of the most used techniques for nonlinear systems, and have been analyzed and implemented within VRFB systems or similar electrochemical systems. However, the main point of HGO and SMO techniques, is the computation of a mathematical map that transforms the system in a certain canonical form, which can be computationally unfeasible for high-order systems. Therefore, in this work it is proposed the design of a nonlinear observer. The estimator has been formulated using Linear Matrix Inequalities (LMI) to compute the observer gains, that can be selected in order to make the observer less sensitive against measurement signals noise.

This paper has been organized as follows: Section 2 presents the problem formulation with the nonlinear model and the OCV expression. Section 3 shows the model reduction based on the conservation principles. In Section 4 the design of the observer by means of LMI formulation is presented. All the study has been validated through numerical simulation in Section 5 and experimentally in Section 6. Finally, Section 7 presents the main conclusions of this work.

2 MODEL FORMULATION

This work is based on the nonlinear electrochemical model developed by Skyllas-Kazacos [21]. This model has been validated in real VRFB systems, being accepted and used in many works for state and parameter estimation purposes [40].

Even though this model presents a great correspondence with a real system, multiple authors impose additional assumptions to simplify the estimator design, and might not be extrapolated in all scenarios. On the one hand, it is common to consider that the electrolyte flow rate q, is the same one in both sides of the system, and large enough to guarantee that the vanadium species concentration in both cells and tanks are equal. On the other hand, all SOC observers proposed use the hypothesis of a balanced system, assuming same concentration in the cathode and the anode sides of the system. These considerations are restrictive and not reasonable in many practical scenarios. It is usual that the flow rates are variable and different in both sides of the system.

In terms of developing a SOC estimator that can be extrapolated to any scenario, where the concentrations of both sides can be different due to the presence of side reactions, the typical assumptions discussed must be obviated.

In this work, the model differentiates between the catholyte and anolyte sides, as well as between the tank and cell parts, without the assumption of large flow rates. Moreover, the diffusion effect has been neglected, introducing a new variable that depicts the system imbalance. In this way, the model presented in this work considers all possible transport phenomena, such as diffusion, migration or convection, without the need to explicitly formulate them mathematically. This is important, because these transport phenomena have very slow dynamics, compared to the ones produced by the effect of flow rates and current, making difficult to differentiate between various effects or even a possible degradation.

With these considerations, the VRFB dynamics can be described through an 8th order model. In order to present it in a more compact form, which also allows to develop observers in a more understandable way, the system dynamics has been rewritten using the state-space formalism. The main benefit of its use is the possibility of formulate the LMIs required to compute the observer gains in an efficient way. Therefore, the system dynamics are formulated as follows:

$$\dot{\boldsymbol{x}} = \mathbf{A}_{-}\boldsymbol{x} \cdot q_{-} + \mathbf{A}_{+}\boldsymbol{x} \cdot q_{+} + \mathbf{b} \cdot j \,, \tag{1}$$

where $\boldsymbol{x} = [c_2^c, c_3^c, c_4^c, c_5^c, c_2^t, c_3^t, c_4^t, c_5^t]^\top$ is the state vector, c_i^k stands for the concentration of vanadium specie V^{i+} in k, with $k = \{c, t\}$ meaning the concentration in the cell and the tank respectively, q_- and q_+ are the flow rates of the anolyte and catholyte parts and j is the current. Matrices $\mathbf{A}_-$ and $\mathbf{A}_+$ are related with the flow rate part, and the vector $\mathbf{b}$ depicts the flux of electrons that appear between the current collectors, making possible the redox reaction inside the cell. Both matrices $\mathbf{A}_+$, $\mathbf{A}_-$ and vector $\mathbf{b}$ appear summarized in the Appendix A2 with their corresponding parameters defined in Table 3 of Appendix A1.

The system output considered in this work is the voltage, which can be computed as the sum of two terms. On the one hand, the Open Circuit Voltage (OCV), which is commonly the most used measurement in VRFB parameter estimation [28]. On the other hand, the overpotential term η, which is structured as the addition of three overpotentials: ohmic, activation and concentration overpotentials.

$$E = \mathrm{OCV} + \eta \ . \tag{2}$$

With respect to the overpotential η, assuming that the battery works in nominal currents operating conditions where the SOC is limited between 20 to 80% [33], the contribution of the concentration and activation overpotentials is very small in comparison to the ohmic overpotential [20]. Therefore, in this work, only the ohmic term is considered:

$$\eta \approx r \cdot j \ , \tag{3}$$

being r the ohmic resistance.

With respect to the OCV, it depends exclusively on the cell concentrations and can be computed by means of the Nernst equation:

$$\mathrm{OCV} = E^{\theta} + \frac{RT}{F} \cdot ln\left(\frac{c_2^c \cdot c_5^c \cdot c_H^2}{c_3^c \cdot c_4^c}\right) \ , \tag{4}$$

where E^{θ} is the standard electrode potential, c_H is the concentration of hydrogen ions, R is the ideal gas constant, T is the electrolyte temperature inside the cell and F is the Faraday constant. From (4) it is possible to split the OCV in two parts differentiating the vanadium and hydrogen concentrations as follows:

$$\mathrm{OCV} = E^{\theta} + \frac{RT}{F} \cdot ln\left(\frac{c_2^c \cdot c_5^c}{c_3^c \cdot c_4^c}\right) + \frac{2RT}{F} \cdot ln\left(c_H\right) \ . \tag{5}$$

As the hydrogen ions concentration is difficult to obtain, it is possible to introduce its weight in the E^{θ} term as follows [19]:

$$E^{\theta'} = E^{\theta} + \frac{2RT}{F} \cdot ln\left(c_H\right) \ , \tag{6}$$

where $E^{\theta'}$ is the sum of the standard electrode potential with the hydrogen ions term. Therefore, it is possible to define the OCV function used in this work as:

$$\mathrm{OCV} = E^{\theta'} + \frac{RT}{F} \cdot ln\left(\frac{c_2^c \cdot c_5^c}{c_3^c \cdot c_4^c}\right) \ . \tag{7}$$

With the model presented in (1), it is possible to formally define the expression of the SOC. In this work, the SOC is defined as follows:

$$\mathrm{SOC} = min\{\mathrm{SOC}_-, \mathrm{SOC}_+\} \ , \tag{8}$$

where SOC_- and SOC_+ are used to define, respectively, the SOC in the anolyte and catholyte sides, with the following expressions:

$$\begin{aligned} \mathrm{SOC}_- &= \left(\frac{c_2^t v_-^t + c_2^c v^c}{c_2^t v_-^t + c_2^c v^c + c_3^t v_-^t + c_3^c v^c}\right) \\ \mathrm{SOC}_+ &= \left(\frac{c_5^t v_+^t + c_5^c v^c}{c_4^t v_+^t + c_4^c v^c + c_5^t v_+^t + c_5^c v^c}\right) \ , \end{aligned} \tag{9}$$

being v^c, v_-^t and v_+^t the cell, anolyte tank and catholyte tank volumes, which are assumed constant and appear defined in Table 2. As it can be noticed, the SOC computation requires the estimation of the species concentration inside the cell. This is a novelty compared to other studies, that assume a negligible volume of the cell with respect to the tanks.

Finally, considering the previous formulations of the model, it is convenient to re-write the system in the following form:

$$\begin{aligned} \dot{\boldsymbol{x}} &= \mathbf{A}_{-}\boldsymbol{x} \cdot q_- + \mathbf{A}_{+}\boldsymbol{x} \cdot q_+ + \mathbf{b} \cdot j \\ y &= h(\boldsymbol{x}) = ln\left(\frac{x_1 \cdot x_4}{x_2 \cdot x_3}\right) \ , \end{aligned} \tag{10}$$

where y is the system output, that corresponds to extract from equation (2) the ohmic overpotential η and from the OCV defined in (7) the parameter $E^{\theta'}$ and the constant factors which are known. Therefore, the system output is a nonlinear function $h(x)$ that depends exclusively on the states. The aim of this work is to propose an observer that is able to estimate these states $\boldsymbol{x}$, and therefore the SOC by means of the equation in (8), using only the measured signal y.

3 MODEL REDUCTION

The studied VRFB model satisfies a set of conservation principles that can be utilized to reduce the dimension of the system and ease the observer design.

3.1 Conservation principles

As the VRFB model presented assumes that there are no losses inside the system, the mass and charge conservation laws can be applied.

On the one hand, according to the mass conservation principle, the total mass of species inside a VRFB must remain constant. In terms of a RFB system, this principle can be extrapolated to the conservation of total number of moles inside the system, which can be computed by means of the following expression:

$$m_t = (c_2^c + c_3^c + c_4^c + c_5^c)v^c + (c_2^t + c_3^t)v_-^t + (c_4^t + c_5^t)v_+^t \ , \tag{11}$$

where m_t represents the total number of moles of vanadium species inside the system. In order to verify that

m_t is constant, it is possible to analyze its dynamics, which can be written as:

$$\dot{m}_t = \boldsymbol{v} \cdot \dot{\boldsymbol{x}} \,, \tag{12}$$

being $\boldsymbol{v}$ the volume vector that takes the form: $\boldsymbol{v} = [v^c, v^c, v^c, v^c, v^t_-, v^t_-, v^t_+, v^t_+]$. Using (1), it can be seen that:

$$\dot{m}_t = 0 \,, \tag{13}$$

which shows that the total vanadium mass is constant.

On the other hand, considering the charge conservation principle, the total charge must be equal along the time. For this case, the expression that express this law for the VRFB system is:

$$\begin{aligned} c_t = {} & (2c^c_2 + 3c^c_3 + 4c^c_4 + 5c^c_5)v^c + (2c^t_2 + 3c^t_3)v^t_- \\ & + (4c^t_4 + 5c^t_5)v^t_+ \,, \end{aligned} \tag{14}$$

where c_t is used to express the total charge of the system, which depends on the valence i of each vanadium species V^{i+}. It is possible to analyze the total charge evolution as:

$$\dot{c}_t = \boldsymbol{v_c} \cdot \dot{\boldsymbol{x}} \,, \tag{15}$$

where in that case the volume vector is $\boldsymbol{v_c} = [2v^c, 3v^c, 4v^c, 5v^c, 2v^t_-, 3v^t_-, 4v^t_+, 5v^t_+]$, obtaining that its value is zero, which means that the total charge remains constant inside the system.

Finally, the imbalance can be included to the system, by means of a third expression that can be extracted from the mass conservation principle. It is possible to express the total mass in one side of the system, in this case it has been considered the catholyte, m_+ by means of the following expression:

$$m_+ = (c^c_4 + c^c_5)v^c + (c^t_4 + c^t_5)v^t_+ \,. \tag{16}$$

By means of this expression, it is also possible to compute the mass in the anolyte side, defined as m_-, as the difference between the total and the catholyte mass.

$$m_- = m_t - m_+ \,. \tag{17}$$

3.2 Reduced model formulation

As expressions (11), (14) and (16) are linearly independent between them, they can be used to reduce the number of states to 5, adding the 3 new known parameters m_t and c_t and the vanadium mass in the catholyte side m_+, that despite not being constant, its value changes very slowly over time.

Therefore, it is possible to reformulate the model choosing the states that will be removed from the original system. In this work, in order to facilitate the observer design, it has been decided to keep the cell states, which appear directly in the system measured output equation. Thus, the tank concentrations c^t_3, c^t_4 and c^t_5 have been the removed ones. Assuming that both flow rates q_- and q_+ are constant, it is possible to formulate the new system dynamics:

$$\begin{aligned} \dot{\bar{\boldsymbol{x}}} &= \bar{\mathbf{A}}\bar{\boldsymbol{x}} + \bar{\mathbf{b}}j + \boldsymbol{\phi}(m_t, c_t, m_+) \\ y &= h(\bar{\boldsymbol{x}}) \end{aligned} \tag{18}$$

where $\bar{\boldsymbol{x}} \in \mathbb{R}^5$ is the reduced dimension state variable, being $\bar{\boldsymbol{x}} = [c^c_2, c^c_3, c^c_4, c^c_5, c^t_2]^\top$, $\bar{\mathbf{A}}$ is the new matrix of flow rate effect, $\bar{\mathbf{b}}$ the current effect vector and $\boldsymbol{\phi}$ is the vector of the new parameters m_t, c_t and m_+ that can be expressed as $\boldsymbol{\phi}(m_t, c_t, m_+)$. All these new matrices are summarized in the Appendix A3.

4 OBSERVER DESIGN

This section will cover the procedure developed to design a nonlinear observer for the nonlinear system presented in (18). Due to the nonlinear nature of the system, the EKF appears as a possible candidate technique [44], but it has some significant drawbacks.

On the one hand, this technique is only a local solution, that is, it only converges if the observer state is initialized near to the real value. In a RFB system, it is difficult to initialize due to the fact that the electrolytes do not provide any variable that can be measured in a simple way and provide information on the species concentration. Therefore, the concentrations are considered totally unknown and it is not possible to ensure that the observer state is near to the real value.

On the other hand, this technique implies a linearization of the system, which may eliminate some properties that can be useful to design an adequate estimator in a more direct way. This is critical in RFB systems, as the model presents a particular property that allows the design of a global nonlinear observer in a direct way.

4.1 System property

A key property to remark is that the main non-linearity of the system, which appears in the in the output function $h(\boldsymbol{x})$, satisfies a bounded jacobian condition. That is,

$$\boldsymbol{k}_{h,1} \leq \frac{\partial h}{\partial \bar{\boldsymbol{x}}} \leq \boldsymbol{k}_{h,2} \,, \tag{19}$$

where $\boldsymbol{k}_{h,1}$ and $\boldsymbol{k}_{h,2}$ are the lower and upper vectors of values that bound the output jacobian.

This fact can be deduced from the following. Considering that the output h is the OCV defined by means of (2), its jacobian computation takes the following form:

$$\frac{\partial h}{\partial \bar{\boldsymbol{x}}} = \begin{bmatrix} \frac{1}{c^c_2} & \frac{-1}{c^c_3} & \frac{-1}{c^c_4} & \frac{1}{c^c_5} & 0 \end{bmatrix}, \tag{20}$$

that fulfills the bounded jacobian condition (19) according to the values of $\boldsymbol{k}_{h,1}$ and $\boldsymbol{k}_{h,2}$ that can be computed as:

$$\begin{aligned} \boldsymbol{k}_{h,1} &= \begin{bmatrix} \frac{1}{c^c_{2,max}} & \frac{-1}{c^c_{3,min}} & \frac{-1}{c^c_{4,min}} & \frac{1}{c^c_{5,max}} & 0 \end{bmatrix} \\ \boldsymbol{k}_{h,2} &= \begin{bmatrix} \frac{1}{c^c_{2,min}} & \frac{-1}{c^c_{3,max}} & \frac{-1}{c^c_{4,max}} & \frac{1}{c^c_{5,min}} & 0 \end{bmatrix} \end{aligned} \tag{21}$$

where $c^c_{i,min}$ and $c^c_{i,max}$ are respectively, the minimum and maximum concentration of vanadium species i.

By fulfilling the bounded jacobian condition, the system model can be rewritten in the following form:

$$\begin{aligned} \dot{\bar{x}} &= \bar{\mathbf{A}}\bar{x} + \bar{\mathbf{b}}j + \boldsymbol{\phi} \\ y &= \boldsymbol{k}_{h,1}\bar{x} + \bar{h}(\bar{x}) \end{aligned} \tag{22}$$

where $\bar{h}(\bar{x})$ is a monotonic function that can be computed as:

$$\bar{h}(\bar{x}) = -\boldsymbol{k}_{h,1}\bar{x} + h(\bar{x}). \tag{23}$$

The main characteristic of a monotonic function is that it always increases or decreases according to the states evolution. For the case of the VRFB system, is always a mononotic non-decreasing function for the case of a charging process, and a monotonic decreasing function for the case of a discharging ones. This monotonic output behaviour, is very useful for developing observers [27] and will be exploited in this work.

4.2 Observer structure

Taking into account the formulation of the new system dynamics fulfilling the bounded jacobian condition (22), the nonlinear observer that is proposed in this study has the following dynamics:

$$\begin{aligned} \dot{\hat{\bar{x}}} = \bar{\mathbf{A}}\hat{\bar{x}} + \boldsymbol{\kappa_1}\left[y - \boldsymbol{k}_{h,1}\hat{\bar{x}} - \bar{h}\left(\hat{\bar{x}} + \boldsymbol{\kappa_2}(y - \boldsymbol{k}_{h,1}\hat{\bar{x}} - \bar{h}(\hat{\bar{x}})\right)\right] \\ + \bar{\mathbf{b}}j + \boldsymbol{\phi}\,, \end{aligned} \tag{24}$$

where $\hat{\bar{x}}$ is the observer state vector, and $\boldsymbol{\kappa_1}$ and $\boldsymbol{\kappa_2}$ are the observer gains in $\mathbb{R}^5$ to be tuned. A scheme of the proposed observer is presented in Figure 2 where it is possible to see how it is composed by a copy of the system dynamics and combination of a linear and a nonlinear feedback term. The main advantage of this structure is that using the property of bounded jacobian the observer can be proved to work in all the operating region, thus, avoids the need of initializing the observer states.

Regarding the design of the gains, there exists a simple computational way to find their values, by means of a LMI [5]. For the present work, these gains must be tuned using the following LMI, that must be fulfilled for some symmetric positive definite matrix $\mathbf{P} \in \mathbb{R}^{5\times5}$ and a vector $\Upsilon \in \mathbb{R}^5$:

$$\begin{bmatrix} \bar{\mathbf{A}}^\top\mathbf{P} + \mathbf{P}\bar{\mathbf{A}} + 2\epsilon\mathbf{P} - \boldsymbol{k}^\top_{h,1}\Upsilon^\top - \Upsilon\boldsymbol{k}_{h,1} & * \\ -\Upsilon & \mathbf{0} \end{bmatrix} - \begin{bmatrix} \mathbf{0} & * \\ -\frac{\boldsymbol{k}_{h,2} - \boldsymbol{k}_{h,1}}{2}\left(\mathbf{I} - \boldsymbol{\kappa_2}\frac{\partial h}{\partial \boldsymbol{x}}\right) & \mathbf{I} \end{bmatrix} < 0 \tag{25}$$

where $*$ denotes the symmetric terms of the respective matrices, $\mathbf{0}$ and $\mathbf{I}$ are the zero and identity matrices of the corresponding dimensions. Then, if the observer gains are tuned as $\boldsymbol{\kappa_1} = \mathbf{P}^{-1}\Upsilon$ and $\boldsymbol{\kappa}_2$ is obtained directly from (25), the estimation error e, defined as $e = (\bar{x} - \hat{\bar{x}})$, will be asymptotically stable satisfying the following condition [35]:

$$\left\|\bar{x}(t) - \hat{\bar{x}}(t)\right\| \leq k\left\|\bar{x}(0) - \hat{\bar{x}}(0)\right\| e^{-\epsilon t}\,, \tag{26}$$

where $\|\cdot\|$ is the norm operation, ϵ is the convergence rate, k is a positive constant and t defines the time. This condition ensures the observer stability, with the advantage of being able to tune the ϵ parameter. Thus, the larger ϵ is, the faster the state will converge to the real value. However, increasing ϵ also increases the noise sensitivity of the observer, so it should be chosen seeking a balance between variance and convergence rate. The proof of the observer stability is presented in the Appendix A4.

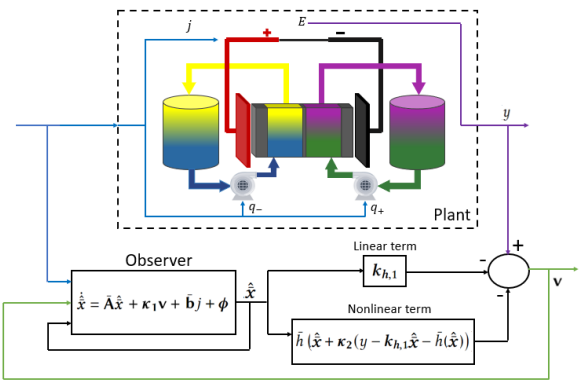

Figure 2: Observer scheme.

5 NUMERICAL SIMULATION

In order to validate the proposed observer, a series of simulations have been carried out to study if it is capable of estimating the states $\bar{x}$, and therefore, the SOC. For this numerical analysis, realistic vanadium concentrations have been considered, with a total vanadium concentration of species in the electrolyte equal to 0.4

M [10]. The other parameters of the system appears summarized in Table 1.

A key-point of the proposed approach is the capability of estimating the internal states considering that the vanadium species concentration can be different in the cell and tank. Therefore, the flow rates that have been chosen in such a way that there is a significant concentration difference between both sides of the system. On the one hand, for the anolyte part, a flow rate $q_- = 5$ ml/min has been chosen, while for the catholyte part has been chosen a lower ones $q_+ = 50$ ml/min.

Figure 3 shows the evolution of the active species V^{2+} and V^{5+} during a constant current charge and discharge cycle, with an absolute value of 1.5 A, assuming an electrolyte temperature of 298 K. Notice that, as the electrolyte flow rate of the catholyte part is high, the difference of concentrations between the cell and the tank for the vanadium species V^{5+} is small. However, for a low flow rate as the ones introduced in the anolyte side, the difference is considerable as can be noticed looking the profiles of c_2^c and c_2^t.

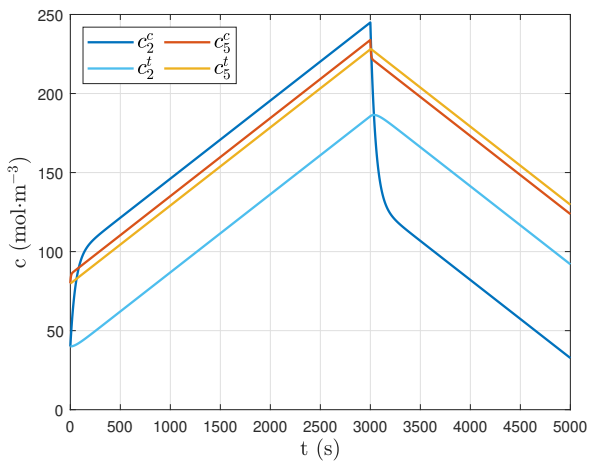

Figure 3: Concentration dynamics of the active species in the system with different flow rates $q_- = 5$ ml/min and $q_+ = 50$ ml/min and a constant charge and discharge current of 1.5 A.

Table 1: Numerical VRFB parameters.

Nomenclature	Value
c_t	0.28 mol e$^-$
m_t	$0.8{\cdot}10^{-2}$ mol
m_+	$0.4{\cdot}10^{-2}$ mol
v^c	$4.5{\cdot}10^{-6}$ m^3
v_-^t	$1{\cdot}10^{-4}$ m^3
v_+^t	$1{\cdot}10^{-4}$ m^3
T	298 K

As it can be noticed, under the proposed flow rates conditions, it is necessary to estimate all states separately, in order to compute the SOC of the system. To do so, the proposed observer in the previous section has been implemented.

Selecting a value of $\epsilon = 0.8$, and considering that the minimum and maximum concentrations of the vanadium species are 0.005 and 0.395 M, the LMI problem defined in (25) can be solved. It is important to remark that the minimum concentration has been considered greater than zero because otherwise it makes not physical sense (negative concentrations can not exist). This consideration has also practical relevance, since for a correct operation of the VRFB, as well as to extend its useful life, it is recommended that the SOC varies between 10 and 90%, without ever reaching null concentrations.

Solving the LMI, the value of the matrix $\mathbf{P}$ and vectors $\boldsymbol{\Upsilon}$ and $\boldsymbol{\kappa_2}$ are:

$$\mathbf{P} = 10^3 \begin{bmatrix} 3.1943 & 2.9537 & 2.2191 & 0.5110 & 1.5224 \\ 2.9537 & 4.3734 & 2.5695 & 0.6362 & 1.8727 \\ 2.2191 & 2.5695 & 2.3021 & 0.6680 & 1.5772 \\ 0.5110 & 0.6362 & 0.6680 & 0.8645 & 0.5121 \\ 1.5224 & 1.8727 & 1.5772 & 0.5121 & 1.9589 \end{bmatrix}$$

$$\boldsymbol{\Upsilon} = \begin{bmatrix} 622.4988 \\ 654.2821 \\ 924.3394 \\ 818.3161 \\ 784.8318 \end{bmatrix} \qquad \boldsymbol{\kappa_2} = \begin{bmatrix} 2.2515 \\ -2.0591 \\ -4.0621 \\ 0.0165 \\ 0.2498 \end{bmatrix}.$$

Finally, the gain $\boldsymbol{\kappa_1}$ can be computed from the above matrices as:

$$\boldsymbol{\kappa_1} = \mathbf{P}^{-1}\boldsymbol{\Upsilon} = \begin{bmatrix} -0.0763 \\ -0.1822 \\ 0.3551 \\ 0.7633 \\ 0.1487 \end{bmatrix}. \tag{27}$$

With these results, the observer has been implemented in order to analyze its robustness and efficiency in terms of SOC estimation. For this purpose, the VRFB dynamics have been initialized with the following initial concentrations $\bar{\boldsymbol{x}}(0) = [40\ 350\ 350\ 40\ 40]^\top$, assuming the system is balanced in its initial moment. On the other hand, the estimation dynamics have been initialized randomly with the following concentrations $\hat{\bar{\boldsymbol{x}}}(0) = [15\ 78\ 24\ 324\ 256]^\top$ assuming there is no information about the system states.

As can be seen in Figure 4, the estimated SOC denoted as $\widehat{\text{SOC}}$ converges to the real ones, which indicates that the designed observer works correctly. As have been explained, increasing the value of ϵ allows to obtain a faster convergence. This can be seen in the same figure where have been plotted the estimated $\widehat{\text{SOC}}$ considering an ϵ of 0.1 and 0.8.

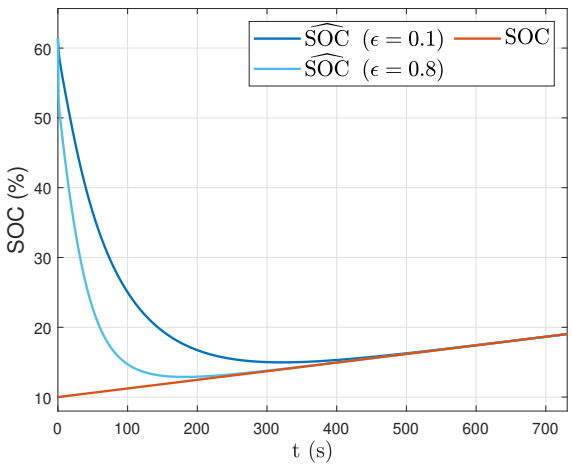

Figure 4: Comparison between the real SOC and the observed ones with different values of ϵ.

In order to analyze the robustness of the observer in term of ϵ, uncertainty and noise have been introduced into the system. On the one hand, the values of the cell volume, v^c, and tank volumes, v^t_+, v^t_-, have been varied, from the ones shown in Table 1 to $5{\cdot}10^{-6}$ m^3 and $0.9{\cdot}10^{-4}$ m^3, respectively. On the other hand, it has been introduced Gaussian distributed noise of variance 0.5 to the OCV measure, which is a significantly large value for the considered system.

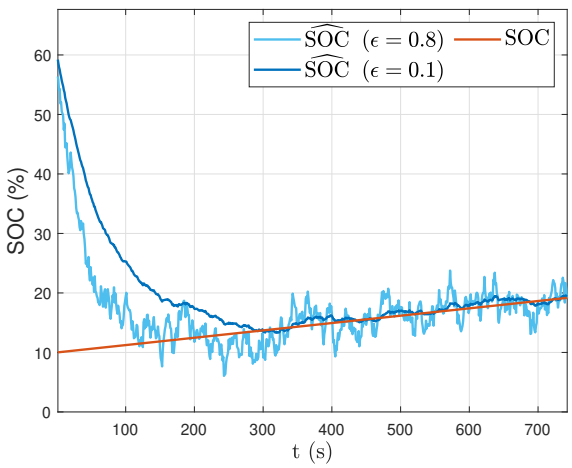

Figure 5: Comparison between the real SOC and the observed ones with different values of ϵ introducing uncertainty and noise inside the system.

As can be noticed in Figure 5, even in the presence of significant measurement noise and model uncertainty, the observer achieves a correct estimation of the SOC. It is possible to see, how due to the system noise and uncertainty, the $\widehat{\text{SOC}}$ with ϵ = 0.8 is more sensitive than the ones of 0.1. Therefore, it is shown how ϵ must be selected searching a trade off between convergence rate and reliability.

Finally, Figure 6 shows the relative error of the estimated $\widehat{\text{SOC}}$ for both cases of ϵ considering the previous noise and uncertainty. It is possible to see that, on the presence of noise and uncertainty in the model parameters, the estimated concentration presents an error of less than 10% for the case of ϵ = 0.1 and peaks of 40% for the case of ϵ = 0.8. It is important to remark, that without the presence of noise and uncertainty (see Figure 4), the observed error is null, making it asymptotically stable according to the procedure develop for the observer design.

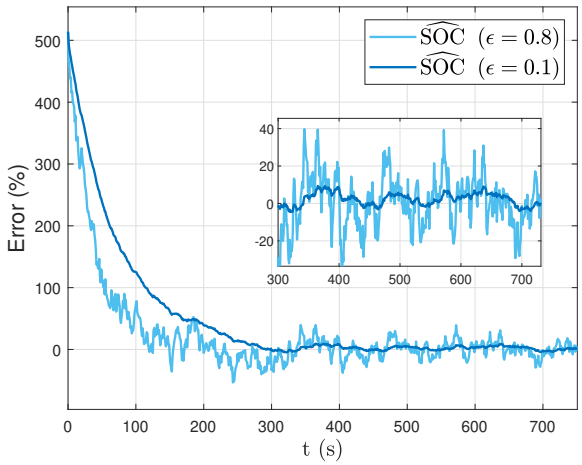

Figure 6: Relative error of the estimated concentration with (red) and without (blue) the consideration of parameter uncertainty and noise.

6 EXPERIMENTAL DESIGN

Once the designed observed has been numerically validated, it has been implemented in a real battery prototype.

6.1 Experimental setup

The experimental VRFB setup is shown in Figure 7 and is composed by a single cell of 25 cm^2 active area developed by the danish company Redox-Flow [1, 23], with a Nafion-117 membrane and 3 mm thick carbon felt electrodes [24]. Through the peristaltic pump BT600L from the Leadfluid manufacturer, the electrolyte flow rates can be monitored and controlled. The tanks used to perform the different experiments have a capacity of 80 ml.

The electrolytes are composed of 1.6 M concentration of vanadium in a solution of sulphuric acid. Initially, there is only a single electrolyte reservoir with

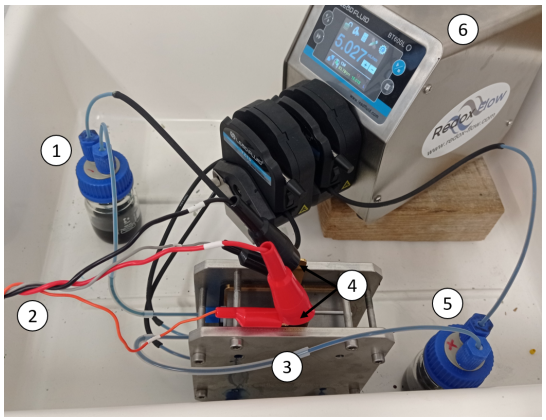

Figure 7: VRFB experimental setup with its main components. 1: Anolyte tank, 2: Current-Voltage sensors, 3: Cell, 4: Current collectors, 5: Catholyte tank, 6: Pump.

a vanadium valence of 3.5, therefore it is necessary to perform a charging process in order to obtain the vanadium species V^{2+} and V^{5+}.

In order to ensure that the vanadium species V^{2+} and V^{5+} are reached, the following procedure has been carried out:

1. Introduce the same quantity of $V^{3.5+}$ electrolyte in the two reservoirs of 80 ml.
2. Charge the battery at a constant current of 2 A until the voltage reaches 1.7 V using flow rates of 5 ml/min.
3. Maintain the battery in charging mode at 1.7 V, allowing a variation in the current value. In this way, the current will decrease until there is no more electrolyte left to react, at which point it is possible to conclude that vanadium species V^{2+} and V^{5+} have been generated.

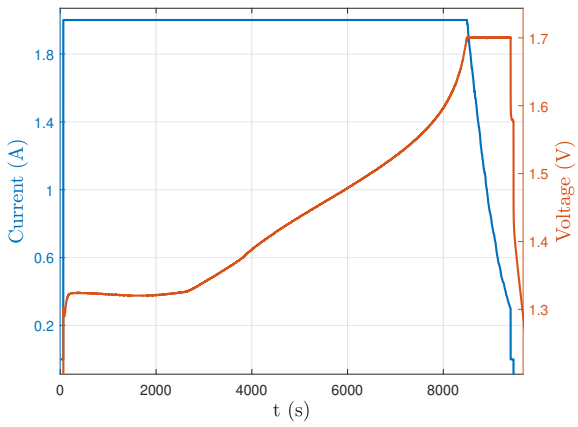

Figure 8: Voltage and current profiles for the generation of vanadium species V^{2+} and V^{5+}.

The profiles of the current and voltage for the generation of the vanadium species is shown in Figure 8. As can be noticed, as soon as the 1.7 V are reached, it is maintained constant and current starts to decrease from 2 to less than 0.4 A. At this point, it is possible to visually identify if the electrolyte has been generated correctly. The nature color of vanadium species V^{5+} is yellow, while the color of V^{2+} is purple, so it can be distinguished from the initial solution that had a bluish color. Figure 9 shows the initial and final colors of the electrolytes obtained from develop the procedure explained. As can be seen, Figure 9a presents the original bluish electrolyte color corresponding to the $V^{3.5+}$, while Figure 9b shows the final electrolytes colors, corresponding to vanadium species V^{2+} and V^{5+}.

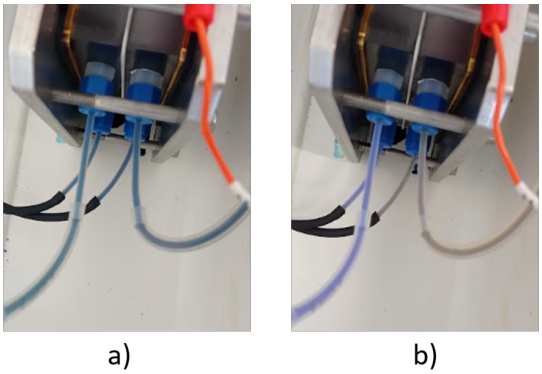

Figure 9: Electrolyte color inside the pipes. At its initial state (a) and at the end of the V^{2+} and V^{5+} generation process (b).

Figure 10 shows the color of the original electrolyte with $V^{3.5+}$ concentration contained in the reservoir, and the V^{5+} obtained from the generation process. In this scenario, it is possible to assume that the system is initially full charged, and therefore the initial concentrations are known.

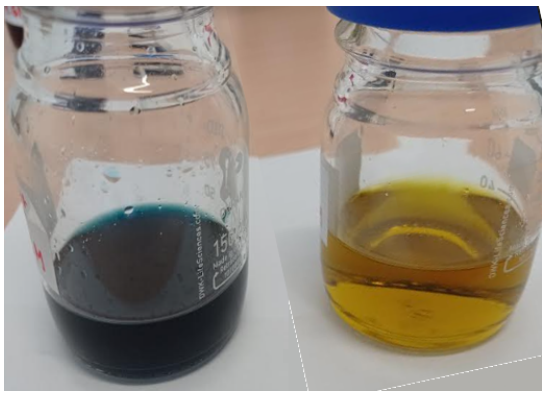

Figure 10: Reservoirs with the original $V^{3.5+}$ electrolyte (left) and the V^{5+} concentration electrolyte (right).

Once the electrolytes for the cathode and anode side of the system have been obtained, it is possible to carry out the different experiments to validate the SOC estimator.

6.2 Model calibration

Before implementing the observer designed to estimate the SOC, first of all it is necessary to calibrate the model. The calibration has been done using a charging process at constant current of 2 A with a constant flow rates of 5 ml/min, after the battery has been partially discharged.

As the total vanadium concentration is 1.6 M, assuming that the system is initially balanced with the same amount of electrolyte of 80 ml in each reservoir, it is possible to compute the value of m_t, c_t and m_+ which appear summarized in Table 2 jointly with the system dimensions.

The parameters that have been estimated to calibrate the model are the ohmic resistance r, the standard electrode potential E^θ and the initial concentrations $\boldsymbol{x}(0)$. In order to relax the problem, it has been assumed that same evolution is presented for the active vanadium species V^{2+} and V^{5+}, and the same for V^{3+} and V^{4+}. Therefore, it is only necessary to estimate the initial concentration inside the tank and cell of one species. In that case, choosing the V^{2+} species, the initial concentration parameters are $c_2^c(0)$ and $c_2^t(0)$.

Using a particle swarm optimization technique [10], it is possible to estimate the set of parameters $\mathbf{p} = [r, E^\theta, c_2^c(0), c_2^t(0)]$, that satisfy the following problem:

$$\begin{aligned} \min_{\mathbf{p}} \quad & \sum_{k=1}^{N} |E(k \cdot T_s) - \hat{E}(k \cdot T_s)| \\ \text{subject to} \quad & \\ & \hat{E}(k \cdot T_s) = f(\mathbf{p}) \\ & \mathbf{p} \in \mathbf{c}(\mathbf{p}) \end{aligned}$$

being N the total number of measures that has been taken, considering a sample period T_s, k denotes each sample, f denotes the cell voltage expressed by (2) as a function of the parameters and $\mathbf{c}$ is the constraint set over the unknown parameters. For the experiment performed, the value of T_s is one second and the constraint set is $\mathbf{c}\ (\mathbf{p}) = [0..1, 0..2, 0..1600, 0..1600]$.

The values of the estimated parameters are presented in Table 2, and the calibrated profile that has been obtained is shown in Figure 11.

As it can be noticed from Figure 11, the calibrated profile of $\hat{E}$ is close to the real E, so the calibration performed by means of the PSO algorithm has achieved good results.

Table 2: Measured and calibrated VRFB parameters.

Nomenclature	Value
c_t	0.896 mol e^-
m_t	0.256 mol
m_+	0.128 mol
v^c	$7.5{\cdot}10^{-6}$ m^3
v_-^t	$8{\cdot}10^{-5}$ m^3
v_+^t	$8{\cdot}10^{-5}$ m^3
T	298 K
r	0.11 Ω
E^θ	1.235 V
$c_2^c(0)$	216.75 mol
$c_2^t(0)$	2.578 mol

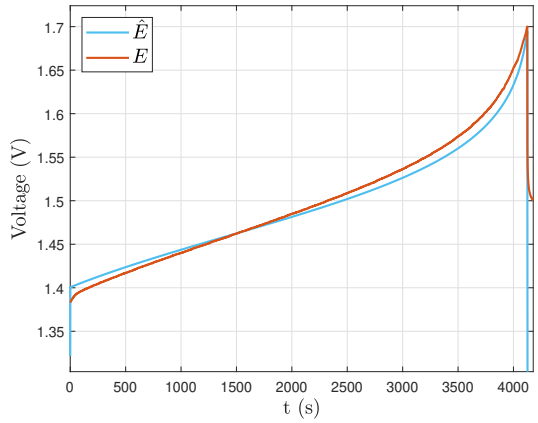

Figure 11: Measured and calibrated profiles of the voltage output.

As a quality estimation measure, the mean squared error (MSE) has been computed, which can be calculated as:

$$MSE = \frac{1}{N} \sum_{k=1}^{N} (E(k \cdot T_s) - \hat{E}(k \cdot T_s))^2$$

obtaining that the MSE value is $3.45{\cdot}10^{-5}$. Therefore, it is possible to guarantee that the model reproduces the real VRFB behavior accurately.

6.3 Results and discussion

Implementing the proposed observer, it is possible to analyze its behaviour in real time. Figure 12 shows the real voltage profile and the estimated ones, obtained with a constant current of 2 A, when the battery is initially full discharged. As can be noticed, the estimation tracks the real value in less than 20 seconds, so the convergence of the states is really fast and accurate.

As the flow rates of 5 ml/min are relatively low for the considered system, it is expected to find a sub-

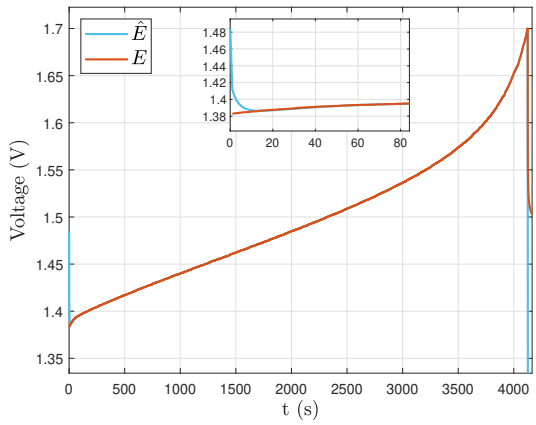

Figure 12: Measured and estimated profiles of the voltage output.

stantial difference between the cell and tank concentrations, as it was shown in Figure 3. In order to analyze this effect, the evolution of c_2^c and c_2^t have been plotted.

Figure 13 shows the evolution of c_2^c and c_2^t where it is possible to see how there exists a clear distinction between cell and tank concentrations due to the low flow rate. Therefore, although the voltage reaches a value of 1.7 V which is obtained when the SOC of the cell is near to the 100 %, the real SOC is near the 80 %. This is because the volume of the tanks is much greater than the one of the cells, and the real SOC of the global system is related with the tank concentrations.

Thus, it is possible to see the effect that generates a low flow rate in the determination of the real SOC of a VRFB, and how assuming cell and tanks concentrations are equal may lead to large estimation errors.

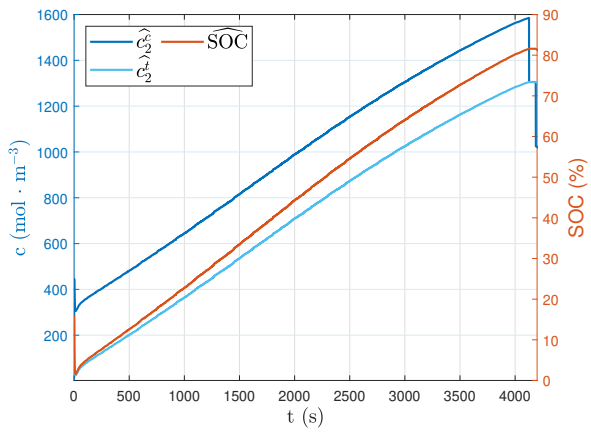

Figure 13: Estimated SOC and cell and tank concentrations of vanadium species V^{2+}.

In order to validate the accuracy of the SOC estimation, a coulomb counting analysis has been performed [25]. The coulomb counting has been obtained integrating the current, which in this case is constant, obtaining a ramp that defines the real SOC of the system, assuming that the initial conditions are known. Its computation depends on the nominal capacity of the battery which can be directly related with the total charge c_t using the Avogadro constant N_A:

$$\mathrm{SOC}(t) = \mathrm{SOC}(0) + \frac{1}{c_t \cdot N_A} \int_0^t j \, dt \tag{28}$$

The drawback of this method, is the requirement of knowing the initial conditions in terms of SOC(0) and the nominal capacity of the system. With respect to the nominal capacity, it is possible to compute its value knowing the total charge of the system, which has been seen is conserved along the time.

With respect to the initial SOC, its value will depend on the distribution of concentrations in each side, accordingly to (9). Therefore, in order to initialize the Coulomb counting method it is necessary to know which are the proportion of concentrations of species to determine the initial SOC(0). Therefore, to get a certain idea of its value, what is commonly done is to take the system to a known operating point, where species concentrations can be approximated with non-significant error. Usually, to determine the initial SOC(0), the operating point that is used is the one corresponding to the end of a charging or discharging process. Therefore, it is possible to initialize the Coulomb counting assuming that the initial SOC(0) is close to 100% or 0%, respectively.

In order to validate the observer presented in this work, it has been considered the case where the system is totally discharged, starting from a 0% SOC. It should be stated, that the proposed observer approach does not need to know the initial conditions of the system.

Figure 14 shows the profile of the measured SOC by means of the coulomb counting technique, the estimated one $\widehat{\mathrm{SOC}}$ and the ones estimated using the cell dynamics and assuming that the concentration in tanks and cells are equal $\widehat{\mathrm{SOC}}_c$.

As can be noticed in Figure 14, the SOC estimation using the assumption of equal concentration in tanks and cells leads to a low accuracy estimation of the real SOC of the system. On the other hand, by means of the proposed observer, the estimation presents a low error compared to the measured value. Comparing the MSE of each case, computing the MSE with the cell SOC leads to 230.56, while for the case of computing the SOC with the proposed observer, its value is only 3.8615 which is low. Therefore, it is possible to verify the correctness of the observer proposed for SOC estimation in cases of low and unequal flow rates.

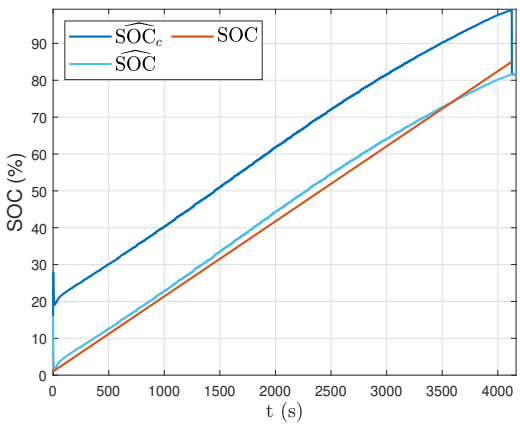

Figure 14: Estimated SOC with low order model ($\widehat{\mathrm{SOC}}_c$), proposed in this work ($\widehat{\mathrm{SOC}}$) and the computed by the coulomb counting (SOC).

7 CONCLUSIONS

This work has presented an observer-based methodology to estimate the SOC of VRFB, proposed methodology combines a nonlinear electrochemical VRFB model and OCV real-time measures. Differently, from previous existing methodologies, in this work it is not assumed cell and tanks concentrations are the same, consequently our method can be applied to wider range of operation conditions.

In order to validate the proposed observer both simulation and experimental analysis have been developed. The experimental results have been validated with a common technique used in the literature to estimate the SOC of any electrochemical system, which consists on the coulomb counting method. Moreover, the proposed technique has been compared with one of the most developed to estimate the SOC of VRFB systems, which consists on the use of a reduced order model. The results show that the use of this novel observer significantly reduces the estimation error, obtaining that the MSE can be reduced a 60% compared to previous observers, in both conditions of different flow rates or low values.

Finding a SOC observer that can handle any flow condition allows it to be used for many purposes such as optimal flow rate control or the development of a voltage controller. However, it is necessary to obtain certain knowledge of the system, in terms of mass imbalance, so a possible future line of work may be the implementation of the observer with an online estimation of the unbalance variable, which would make it possible not to treat it as a parameter, but as a very slow dynamic variable.

Acknowledgements

This research has received the support from the CSIC program for the Spanish Recovery, Transformation and Resilience Plan funded by the Recovery and Resilience Facility of the European Union, established by the Regulation (EU) 2020/2094, CSIC Interdisciplinary Thematic Platform (PTI+) Transicion Energetica Sostenible+ (PTI-TRANSENER+ project TRE2103000), the Spanish Ministry of Science and Innovation under projects MAFALDA (PID2021-126001OB-C31 funded by MCIN/AEI/ 10.13039/501100011033 / ERDF,EU), and MASHED (TED2021-129927B-I00), and by the Spanish Ministry of Universities funded by the European Union - NextGenerationEU (2022UPC-MSC-93823).

APPENDIX

A1. Model parameters

Table 3: VRFB model parameters and constants

Parameter	Meaning (Units)
c_t	Total charge of the system (C)
j	Current (A)
q_-	Anolyte flow rate ($m^3 \cdot s^{-1}$)
q_+	Catholyte flow rate ($m^3 \cdot s^{-1}$)
m_t	Number of moles (mol)
m_+	Number of moles in the catholyte (mol)
v^c	Cell volume (m^3)
v^t_-	Anolyte tank volume (m^3)
v^t_+	Catholyte tank volume (m^3)
F	Faraday constant (96 485 $A \cdot s \cdot mol^{-1}$)
R	Ideal gas constant (8.311 $J \cdot mol^{-1} \cdot K^{-1}$)
T	Electrolyte temperature (298 K)

A2. Original model matrices and vectors

$$\mathbf{A}_- = \begin{bmatrix} -\frac{1}{v^c} & 0 & 0 & 0 & \frac{1}{v^c} & 0 & 0 & 0 \\ 0 & -\frac{1}{v^c} & 0 & 0 & 0 & \frac{1}{v^c} & 0 & 0 \\ 0 & 0 & 0 & 0 & 0 & 0 & 0 & 0 \\ 0 & 0 & 0 & 0 & 0 & 0 & 0 & 0 \\ \frac{1}{v^t_-} & 0 & 0 & 0 & -\frac{1}{v^t_-} & 0 & 0 & 0 \\ 0 & \frac{1}{v^t_-} & 0 & 0 & 0 & -\frac{1}{v^t_-} & 0 & 0 \\ 0 & 0 & 0 & 0 & 0 & 0 & 0 & 0 \\ 0 & 0 & 0 & 0 & 0 & 0 & 0 & 0 \end{bmatrix}$$

$$\mathbf{A}_+ = \begin{bmatrix} 0 & 0 & 0 & 0 & 0 & 0 & 0 & 0 \\ 0 & 0 & 0 & 0 & 0 & 0 & 0 & 0 \\ 0 & 0 & -\frac{1}{v^c} & 0 & 0 & 0 & \frac{1}{v^c} & 0 \\ 0 & 0 & 0 & -\frac{1}{v^c} & 0 & 0 & 0 & \frac{1}{v^c} \\ 0 & 0 & 0 & 0 & 0 & 0 & 0 & 0 \\ 0 & 0 & 0 & 0 & 0 & 0 & 0 & 0 \\ 0 & 0 & \frac{1}{v_+^t} & 0 & 0 & 0 & -\frac{1}{v_+^t} & 0 \\ 0 & 0 & 0 & \frac{1}{v_+^t} & 0 & 0 & 0 & -\frac{1}{v_+^t} \end{bmatrix}$$

$$\mathbf{b} = \frac{1}{F \cdot v^c} \begin{bmatrix} 1 & -1 & -1 & 1 & 0 & 0 & 0 & 0 \end{bmatrix}^\top$$

A3. Reduced model matrices and vectors

$$\bar{\mathbf{A}} = \frac{1}{v^c} \begin{bmatrix} a_{11}v^c & 0 & a_{13}v^c & a_{14}v^c & q_- \\ 0 & a_{22}v^c & a_{23}v^c & a_{24}v^c & -q_- \\ 0 & 0 & -2q_+ & -q_+ & -q_+ \\ 0 & 0 & 0 & -q_+ & q_+ \\ 0 & 0 & 0 & \frac{v^c}{v_+^t}q_+ & -\frac{v^c}{v_+^t}q_+ \end{bmatrix}$$

$$\bar{\mathbf{b}} = \frac{s_e}{F \cdot v^c} \begin{bmatrix} 1 & -1 & -1 & 1 & 0 \end{bmatrix}^\top$$

$$\boldsymbol{\phi} = \frac{1}{v^c} \begin{bmatrix} \left(\frac{3m_t}{v_-^t} + \frac{4m_+}{v^c} - \frac{3m_+v_+^t}{v^cv_-^t} - \frac{c_t}{v_-^t}\right) q_- \\ \left(\frac{c_t}{v_-^t} + \frac{2m_+v_+^t}{v^cv_-^t} - \frac{2m_t}{v_-^t} - \frac{4m_+}{v^c}\right) q_- \\ \frac{m_+}{v^c} q_+ \\ 0 \\ 0 \end{bmatrix}$$

$$a_{11} = \left(-\frac{1}{v^c} - \frac{1}{v_-^t}\right) q_- \quad a_{13} = \left(\frac{1}{v_-^t} + \frac{3v_+^t}{v^cv_-^t} - \frac{4}{v^c}\right) q_-$$

$$a_{14} = \left(\frac{1}{v_-^t} + \frac{3v_+^t}{v^cv_-^t} - \frac{4}{v^c}\right) q_- \quad a_{22} = \left(-\frac{1}{v^c} - \frac{1}{v_-^t}\right) q_-$$

$$a_{23} = \left(\frac{4}{v^c} - \frac{2}{v_-^t} - \frac{2v_+^t}{v^cv_-^t}\right) q_- \quad a_{24} = a_{23} - \left(\frac{1}{v_-^t}\right) q_-$$

A4. Observer proof

Considering the system represented in (24), the dynamics of the estimation error $e = (\bar{x} - \hat{\bar{x}})$ takes the following form:

$$\dot{e} = (\bar{\mathbf{A}} - \boldsymbol{\kappa_1}\boldsymbol{k}_{h,1})e - \boldsymbol{\kappa_1}[\bar{h}(\bar{x}) - \bar{h}(\hat{\bar{x}} + \boldsymbol{\kappa_2}(h(\bar{x}) - h(\hat{\bar{x}}))] \ ,$$

that can be expressed in a more compact way as:

$$\dot{e} = (\bar{\mathbf{A}} - \boldsymbol{\kappa_1}\boldsymbol{k}_{h,1})e - \boldsymbol{\kappa_1}\psi, \tag{29}$$

being ψ a time-varying function of e. This can be proved by means of the mean value theorem, that makes possible to express ψ as [36]:

$$\begin{aligned} \psi &= \bar{h}(\bar{x}) - \bar{h}(\hat{\bar{x}} + \boldsymbol{\kappa_2}(h(\bar{x}) - h(\hat{\bar{x}})) \\ &= \left(\frac{\partial h}{\partial \bar{x}} - \boldsymbol{k}_{h,1}\right)\left(\mathbf{I} - \boldsymbol{\kappa_2}\frac{\partial h}{\partial \bar{x}}\right)(\bar{x} - \hat{\bar{x}}) \ . \end{aligned} \tag{30}$$

Considering also the bounded jacobian property of the output, as it is shown in (19), it is possible to obtain the following constraint:

$$\psi^\top \left[\psi - (\boldsymbol{k}_{h,2} - \boldsymbol{k}_{h,1})\left(\mathbf{I} - \boldsymbol{\kappa_2}\frac{\partial h}{\partial \bar{x}}\right) e\right] \leq 0 \ . \tag{31}$$

By means of this formulation, the system constitutes a Lur'e-system representation. Taking $\mathbf{V}$ as a Lyapunov function candidate for the error dynamics presented in (29), if $\mathbf{V}$ has the form:

$$\mathbf{V} = e^\top \mathbf{P} e, \quad \mathbf{P} > 0 \ , \tag{32}$$

and satisfies the following inequality:

$$\dot{\mathbf{V}} + 2\epsilon\mathbf{V} \leq 0 \ , \tag{33}$$

then, the exponential stability condition expressed by means of (26) is fulfilled [17]. As the left side of (25) takes the following quadratic form:

$$\begin{bmatrix} e \\ \psi \end{bmatrix}^\top \begin{bmatrix} \bar{\mathbf{A}}^\top\mathbf{P} + \mathbf{P}\bar{\mathbf{A}} + 2\epsilon\mathbf{P} & * \\ -\boldsymbol{\kappa_1}^\top\mathbf{P} & \mathbf{0} \end{bmatrix} \begin{bmatrix} e \\ \psi \end{bmatrix} \tag{34}$$

and by considering the condition for e and ψ computed in (31) it is possible to obtain the semidefinite constraints of the LMI formulation presented in (25) applying the S-Procedure [30], that makes asymptotically stable the error e if the gain values of $\boldsymbol{\kappa_1}$ and $\boldsymbol{\kappa_2}$ are correctly tuned.

References

[1] Redox-flow. `https://redox-flow.com`, accessed: 2022-07-20

[2] Anderson, J.L., Moré, J.J., Puleston, P.F., Costa-Castelló, R.: Fuel cell module control based on switched/time-based adaptive super-twisting algorithm: Design and experimental validation. IEEE Transactions on Control Systems Technology pp. 1–8 (2022), `doi:10.1109/TCST.2022.3169441`

[3] Anderson, J.L., Moré, J., Puleston, P., Roda, V., Costa-Castelló, R.: Control super-twisting con

adaptación basada en cruce por cero. análisis de estabilidad y validación. Revista Iberoamericana de Automática e Informática industrial (jul 2022), doi:10.4995/riai.2022.17214

[4] Arenas, L.A., Ponce de León, C., Walsh, F.C.: Redox flow batteries for energy storage: their promise, achievements and challenges. Current Opinion in Electrochemistry **16**, 117–126 (07 2019), doi:10.1016/j.coelec.2019.05.007

[5] Boyd, S., Vandenberghe, L.: Convex Optimization. Cambridge University Press (March 2004)

[6] Cecilia, A., Costa-Castelló, R.: Observador de alta ganancia con zona muerta ajustable para estimar la saturación de agua líquida en pilas de combustible tipo pem. Revista Iberoamericana de Automática e Informática industrial **17**(2), 169–180 (2020), doi:10.4995/riai.2020.12689

[7] Cecilia, A., Sahoo, S., Dragičević, T., Costa-Castelló, R., Blaabjerg, F.: Detection and mitigation of false data in cooperative dc microgrids with unknown constant power loads. IEEE Transactions on Power Electronics **36**(8), 9565–9577 (2021), doi:10.1109/TPEL.2021.3053845

[8] Cecilia, A., Serra, M., Costa-Castelló, R.: Nonlinear adaptive observation of the liquid water saturation in polymer electrolyte membrane fuel cells. Journal of Power Sources **492**, 229641 (2021), doi:10.1016/j.jpowsour.2021.229641

[9] Clemente, A., Cecilia, A., Costa-Castelló, R.: Soc and diffusion rate estimation in redox flow batteries: An i&i-based high-gain observer approach. 20th European Control Conference, Rotterdam **20**, 169–180 (20210)

[10] Clemente, A., Montiel, M., Barreras, F., Lozano, A., Costa-Castelló, R.: Vanadium redox flow battery state of charge estimationusing a concentration model and a sliding mode observer. IEEE Access **9**, 72368–72376 (2021), doi:10.1109/ACCESS.2021.3079382

[11] Clemente, A., Ramos, G., Costa-Castelló, R.: Voltage h∞ control of a vanadium redox flow battery. Electronics **9**, 1567 (09 2020), doi:10.3390/electronics9101567

[12] Clemente, A., Costa-Castelló, R.: Redox flow batteries: A literature review oriented to automatic control. Energies **13**, 4514 (09 2020), doi:10.3390/en13174514

[13] Fornaro, P., Puleston, T., Puleston, P., Serra-Prat, M., Costa-Castelló, R., Battaiotto, P.: Redox flow battery time-varying parameter estimation based on high-order sliding mode differentiators. International Journal of Energy Research (07 2022), doi:10.1002/er.8319

[14] Hall, D., Grenier, J., Duffy, T., Lvov, S.N.: The energy storage density of redox flow battery chemistries: a thermodynamic analysis. Journal of The Electrochemical Society **11**, 117–126 (07 2020), doi:10.1149/1945-7111/aba4e2

[15] Karrech, A., Regenauer-Lieb, K., Abbassi, F.: Vanadium flow batteries at variable flow rates. Journal of Energy Storage **45**, 103623 (2022), doi:10.1016/j.est.2021.103623

[16] Khaki, B., Das, P.: Voltage loss and capacity fade reduction in vanadium redox battery by electrolyte flow control. Electrochimica Acta **405**, 139842 (2022), doi:10.1016/j.electacta.2022.139842

[17] Khalil, H.: Nonlinear systems. Prentice Hall, Upper Saddle River, NJ, USA, **3** (2002)

[18] Knehr, K., Kumbur, E.: Open circuit voltage of vanadium redox flow batteries: Discrepancy between models and experiments. Electrochemistry Communications **13**(4), 342–345 (2011), doi:10.1016/j.elecom.2011.01.020

[19] Knehr, K., Kumbur, E.: Open circuit voltage of vanadium redox flow batteries: Discrepancy between models and experiments. Electrochemistry Communications **13**(4), 342–345 (2011), doi:10.1016/j.elecom.2011.01.020

[20] Langner, J., Melke, J., Ehrenberg, H., Roth, C.: Determination of overpotentials in all vanadium redox flow batteries. ECS Transactions **58**(37), 1 (apr 2014), doi:10.1149/05837.0001ecst

[21] Li, Y., Sun, L., Cao, L., Bao, J., Skyllas-Kazacos, M.: Dynamic model based membrane permeability estimation for online soc imbalances monitoring of vanadium redox flow batteries. Journal of Energy Storage **39**, 102688 (2021), doi:10.1016/j.est.2021.102688

[22] Luna, J., Costa-Castelló, R., Strahl, S.: Chattering free sliding mode observer estimation of liquid water fraction in proton exchange membrane fuel cells. Journal of the Franklin Institute **357**(18), 13816 – 13833 (2020), doi:10.1016/j.jfranklin.2020.10.010

[23] Østedgaard Munck, D.N., Catalano, J., Bentien, A.: Steady state and dynamic response of voltage-operated membrane gates. Membranes **9**(3) (2019), doi:10.3390/membranes9030034

[24] Østedgaard Munck, D.N., Catalano, J., Birch Kristensen, M., Bentien, A.: Data on flow cell optimization for membrane-based electrokinetic energy conversion. Data in Brief **15**, 1–11 (2017), doi:10.1016/j.dib.2017.08.036

[25] Ndeche, K., Ezeonu, S.: Implementation of coulomb counting method for estimating the state of charge of lithium-ion battery. Physical Science International Journal **25**, 1–8 (2021), doi:10.9734/psij/2021/v25i330244

[26] Puleston, T., Clemente, A., Costa-Castelló, R., Serra, M.: Modelling and estimation of vanadium redox flow batteries: A review. Batteries **8**(9) (2022), doi:10.3390/batteries8090121

[27] Rajamani, R., Jeon, W., Movahedi, H., Zemouche, A.: On the need for switched-gain observers for non-monotonic nonlinear systems. Automatica **114**, 108814 (2020), doi:10.1016/j.automatica.2020.108814

[28] Ren, Z., Du, C., Wu, Z., Shao, J., Deng, W.: A comparative study of the influence of different open circuit voltage tests on model-based state of charge estimation for lithium-ion batteries. International Journal of Energy Research **45**(9), 13692–13711 (2021), doi:10.1002/er.6700

[29] Rychcik, M., Skyllas-Kazacos, M.: Characteristics of a new all-vanadium redox flow battery. Journal of Power Sources **22**(1), 59–67 (1988), doi:10.1016/0378-7753(88)80005-3

[30] Scherer, C., Weiland, S.: Lecture notes disc course on linear matrix inequalities in control (2005)

[31] Shin, K.H., Jin, C.S., So, J.Y., Park, S.K., Kim, D.H., Yeon, S.H.: Real-time monitoring of the state of charge (soc) in vanadium redox-flow batteries using uv–vis spectroscopy in operando mode. Journal of Energy Storage **27**, 101066 (2020), doi:10.1016/j.est.2019.101066

[32] Skyllas-Kazacos, M., Kazacos, M.: State of charge monitoring methods for vanadium redox flow battery control. Journal of Power Sources **196**(20), 8822 – 8827 (2011), doi:10.1016/j.jpowsour.2011.06.080

[33] Sánchez-Díez, E., Ventosa, E., Guarnieri, M., Trovò, A., Flox, C., Marcilla, R., Soavi, F., Mazur, P., Aranzabe, E., Ferret, R.: Redox flow batteries: Status and perspective towards sustainable stationary energy storage. Journal of Power Sources **481**, 228804 (2021), doi:10.1016/j.jpowsour.2020.228804

[34] Trovo, A.: Battery management system for industrial-scale vanadium redox flow batteries: Features and operation. Journal of Power Sources **465**(4), 228–229 (2020), doi:10.1016/j.jpowsour.2020.228229

[35] Wang, Y., Rajamani, R.: Feasibility analysis of the bilinear matrix inequalities with an application to multi-objective nonlinear observer design. IEEE 55th Conference on Decision and Control (CDC) **55**, 3252–3257 (2016), doi:10.1109/CDC.2016.7798758

[36] Wang, Y., Rajamani, R., Bevly, D.M.: Observer design for differentiable lipschitz nonlinear systems with time-varying parameters. Proceedings of 53rd IEEE Conference on Decision and Control (CDC) **53** (2014), doi:10.1109/CDC.2014.7039373

[37] Wei, Z., Dong, G., Zhang, X., Pou, J., Quan, Z., He, H.: Noise-immune model identification and state-of-charge estimation for lithium-ion battery using bilinear parameterization. IEEE Transactions on Industrial Electronics **68**(1), 312–323 (2021), doi:10.1109/TIE.2019.2962429

[38] Wei, Z., Hu, J., He, H., Yu, Y., Marco, J.: Embedded distributed temperature sensing enabled multistate joint observation of smart lithium-ion battery. IEEE Transactions on Industrial Electronics **70**(1), 555–565 (2023), doi:10.1109/TIE.2022.3146503

[39] Wei, Z., Hu, J., Li, Y., He, H., Li, W., Sauer, D.U.: Hierarchical soft measurement of load current and state of charge for future smart lithium-ion batteries. Applied Energy **307**, 118246 (2022), doi:10.1016/j.apenergy.2021.118246

[40] Wei, Z., Lim, T.M., Skyllas-Kazacos, M., Wai, N., Tseng, K.J.: Online state of charge and model parameter co-estimation based on a novel multi-timescale estimator for vanadium redox flow battery. Applied Energy **172**, 169–179 (2016), doi:10.1016/j.apenergy.2016.03.103

[41] Wei, Z., Tseng, K.J., Wai, N., Lim, T.M., Skyllas-Kazacos, M.: Adaptive estimation of state of charge and capacity with online identified battery model for vanadium redox flow battery. Journal of Power Sources **332**, 389 – 398 (2016), doi:10.1016/j.jpowsour.2016.09.123

[42] Xiong, B., Zhao, J., Su, Y., Wei, Z., Skyllas-Kazacos, M.: State of charge estimation of vanadium redox flow battery based on sliding mode observer and dynamic model including capacity fading factor. IEEE Transactions

on Sustainable Energy **8**(4), 1658–1667 (2017), doi:10.1109/TSTE.2017.2699288

[43] Xiong, B., Zhang, H., Deng, X., Tang, J.: State of charge estimation based on sliding mode observer for vanadium redox flow battery. In: 2017 IEEE Power Energy Society General Meeting. pp. 1–5 (2017), doi:10.1109/PESGM.2017.8274042

[44] Xiong, B., Zhao, J., Wei, Z., Skyllas-Kazacos, M.: Extended kalman filter method for state of charge estimation of vanadium redox flow battery using thermal-dependent electrical model. Journal of Power Sources **262**, 50 – 61 (2014), doi:10.1016/j.jpowsour.2014.03.110

[45] Zhang, Y., Zhao, J., Wang, P., Skyllas-Kazacos, M., Xiong, B., Badrinarayanan, R.: A comprehensive equivalent circuit model of all-vanadium redox flow battery for power system analysis. Journal of Power Sources **290**, 14–24 (2015), doi:10.1016/j.jpowsour.2015.04.169